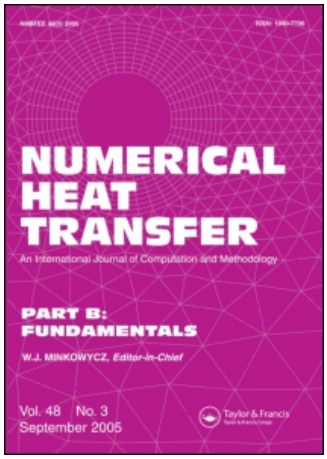

Numerical Heat Transfer, Part B: Fundamentals
An International Journal of Computation and Methodology
Publication details, including instructions for authors and subscription information:
http://www.informaworld.com/smpp/title~content=t713723316

Multidomain Thermal Simulation of CNT Composites by Hybrid BNM

Jianming Zhang [a]
[a] State Key Laboratory of Advanced Design and Manufacturing for Vehicle Body, College of Mechanical and Automotive Engineering, Hunan University, Changsha, People's Republic of China

Online Publication Date: 01 March 2008
To cite this Article: Zhang, Jianming (2008) 'Multidomain Thermal Simulation of CNT Composites by Hybrid BNM', Numerical Heat Transfer, Part B: Fundamentals, 53:3, 246 - 258
To link to this article: DOI: 10.1080/10407790701790176
URL: http://dx.doi.org/10.1080/10407790701790176

Numerical Heat Transfer, Part B, 53: 246–258, 2008

ISSN: 1040-7790 print/1521-0626 online
DOI: 10.1080/10407790701790176

MULTIDOMAIN THERMAL SIMULATION OF CNT COMPOSITES BY HYBRID BNM

Jianming Zhang
State Key Laboratory of Advanced Design and Manufacturing for Vehicle Body, College of Mechanical and Automotive Engineering, Hunan University, Changsha, People's Republic of China

The equivalent heat conductivity of the carbon nanotube (CNT)-reinforced nanocomposites is evaluated using a representative volume element (RVE) with one or several CNTs embedded. The hybrid boundary method (hybrid BNM) is combined with a multidomain solver to analyze the RVE with proper boundary conditions. Some preliminary results are presented and discussed. Emphasis is placed on studying the impact of the CNT's alignment on the equivalent thermal properties. It is demonstrated that the equivalent thermal properties are strongly dependent on the CNT's alignment. Some specific alignments may significantly increase the equivalent heat conductivity of the CNT composites. The feasibility of the method for further investigation is also demonstrated.

1. INTRODUCTION

Since their discovery over a decade ago, carbon nanotubes (CNTS) have been attracting considerable attentions from both scientists and engineers. Intensive research has been carried out on these quasi-one-dimensional structures for their production, physical properties, and possible applications [1, 2]. Numerous remarkable physical properties have been reported for this new form of carbon structure through theoretical and experimental investigations. For example, in addition to the mechanical properties, for which the stiffness, strength, and resilience exceed any current materials, values of thermal conductivity ranging from 1,750 to 5,850 W/m K were obtained from a few recent experiments conducted on mats of compressed ropes of CNTs [3, 4]. Following those experiments, several molecular dynamics (MD) simulations of the thermal conductivity gave even higher values, namely, 6,600 W/m K at 300 K [5]. Although the estimated values were different from one another, it is generally accepted that the CNTs possess excellent heat conductivity, comparable or even better than diamond, considered so far as the best heat conductor in the world.

Received 4 April 2007; accepted 10 October 2007.
This work is supported by the National 973 Program under Grant 2004CB719402 and the program for New Century Excellent Talents in University (NCET-04-0766).
Address correspondence to Jianming Zhang, College of Mechanical and Automotive Engineering, Hunan University, Changsha, 410082, People's Republic of China. E-mail: zhangjianm@gmail.com

The exceptional properties make carbon nanotubes promising in engineering applications, such as development of fundamentally new composite materials, and heat transport management in miniature device components. CNT-based composites offer significant improvements to performance over their base polymers. It has been demonstrated that with only 1% (by weight) of CNTs added to a matrix material, the stiffness of a resulting composite can increase as much as 36–42% and the tensile strength up to 25% [6].

Numerical simulation can help on the understanding, analysis, and design of such nanocomposites. Simulations of individual CNTs using atomistic or molecular dynamics models have provided abundant results, helping in understanding their thermal, mechanical, and electrical behavior. However, these simulations are so far limited to very small length and time scales and cannot deal with the larger models, mainly because of the limitations of current computing power. Continuum mechanics has also been successfully applied for individual CNTs or CNT bundles to investigate their mechanical properties. Although the validity of the continuum approach to modeling of CNTs is still not fully confirmed and will continue to be questioned, it seems at present to be the only feasible approach for carrying out some preliminary simulations of CNT-based composites.

The issue of nanotube dispersion in the host matrix is critical to efficient reinforcement. It is tested that alignment of single-walled nanotubes (SWNTs) increases the parallel components of both the electrical and thermal conductivities with respect to unoriented material. Many attempts have been made to fabricate materials with a controllable degree of CNT alignment. These methods include mechanical stretching [7], magnetic alignment [8], and electrospinning processes [9]. In this article, we focus on investigating the impact of the CNT's alignment on the thermal properties through numerical simulation. The multidomain hybrid boundary method (hybrid BNM) is first developed. The equivalent heat conductivity of carbon nanotube-based composites is evaluated using a representative volume element (RVE) based on 3-D potential theory and solved by means of the multidomain hybrid BNM. Three RVEs containing one, two, and four nanotubes, respectively, have been studied in detail. It was realized that some specific alignments may significantly increase the equivalent heat conductivity of the nanocomposites.

2. MULTIDOMAIN HYBRID BNM

Even with a continuum approach, simulation of the heat-conducting behavior of the CNT-based composites using standard numerical solution techniques such as the finite-element method (FEM) or the boundary-element method (BEM) may face severe difficulties in discretization of the domain geometry. To alleviate this difficulty the hybrid boundary node method [10–14] can be used. By combining a modified functional with the moving-least-squares (MLS) approximation, the hybrid BNM is a truly meshless, boundary-only method. In fact, the hybrid BNM requires only discrete nodes located on the surface of the domain and its parametric representation. As the parametric representation of created geometry is used in all computer aided design (CAD) packages, it should be possible to exploit their open architecture features and handle truly arbitrary geometries. In this section, formulations for the

multidomain hybrid BNM are given. For full details of the single-domain hybrid BNM for 3-D potential problems, refer to [14].

Suppose that n carbon nanotubes are distributed in a polymer matrix which makes an RVE. It is assumed that both the CNTs and the matrix in the RVE are continua of linear, isotropic, and homogenous materials with given heat conductivities. A steady-state heat conduction problem governed by Laplace's equation with proper boundary conditions is considered for each CNT domain and the matrix domain.

The hybrid boundary node method is based on a modified variational principle, in which there are three independent variables:

Temperature within the domain, ϕ
Boundary temperature, $\tilde{\phi}$
Boundary normal heat flux, $\tilde{q}$

Suppose that N nodes are randomly distributed on the bounding surface of a single domain. The domain temperature is approximated using fundamental solutions as

$$\phi = \sum_{I=1}^{N} \phi_I^s x_I \tag{1}$$

and hence, at a boundary point, the normal heat flux is given by

$$q = -\kappa \sum_{I=1}^{N} \frac{\partial \phi_I^s}{\partial n} x_I \tag{2}$$

where ϕ_I^s is the fundamental solution with the source at a node $\mathbf{s}_I$, κ is the heat conductivity, and x_I are unknown parameters. For 3-D steady-state heat conduction problems, the fundamental solution can be written as

$$\phi_I^s = \frac{1}{\kappa} \frac{1}{4\pi r(Q, \mathbf{s}_I)} \tag{3}$$

where Q is a field point; $r(Q, \mathbf{s}_I)$ is the distance between the point Q and the node $\mathbf{s}_I$.

The boundary temperature and normal heat flux are interpolated by moving-least-squares (MLS) approximation:

$$\tilde{\phi}(\mathbf{s}) = \sum_{I=1}^{N} \Phi_I(\mathbf{s}) \hat{\phi}_I \tag{4}$$

and

$$\tilde{q}(\mathbf{s}) = \sum_{I=1}^{N} \Phi_I(\mathbf{s}) \hat{q}_I \tag{5}$$

In the foregoing equations, $\Phi_I(\mathbf{s})$ is the shape function of the MLS approximation; $\hat{\phi}_I$ and $\hat{q}_I$ are nodal values of temperature and normal flux, respectively.

For the polymer domain, the following set of hybrid BNM equations can be written:

$$\begin{bmatrix} \boldsymbol{U}_{00}^{p} & \boldsymbol{U}_{01}^{p} & \cdots & \boldsymbol{U}_{0n}^{p} \\ \boldsymbol{U}_{10}^{p} & \boldsymbol{U}_{11}^{p} & \cdots & \boldsymbol{U}_{1n}^{p} \\ \vdots & \vdots & \ddots & \vdots \\ \boldsymbol{U}_{n0}^{p} & \boldsymbol{U}_{n1}^{p} & \cdots & \boldsymbol{U}_{nn}^{p} \end{bmatrix} \begin{Bmatrix} \boldsymbol{x}_0^p \\ \boldsymbol{x}_1^p \\ \vdots \\ \boldsymbol{x}_n^p \end{Bmatrix} = \begin{Bmatrix} \boldsymbol{H}_0^p \hat{\boldsymbol{\phi}}_0^p \\ \boldsymbol{H}_1^p \hat{\boldsymbol{\phi}}_1^p \\ \vdots \\ \boldsymbol{H}_n^p \hat{\boldsymbol{\phi}}_n^p \end{Bmatrix} \tag{6}$$

$$\begin{bmatrix} \boldsymbol{V}_{00}^{p} & \boldsymbol{V}_{01}^{p} & \cdots & \boldsymbol{V}_{0n}^{p} \\ \boldsymbol{V}_{10}^{p} & \boldsymbol{V}_{11}^{p} & \cdots & \boldsymbol{V}_{1n}^{p} \\ \vdots & \vdots & \ddots & \vdots \\ \boldsymbol{V}_{n0}^{p} & \boldsymbol{V}_{n1}^{p} & \cdots & \boldsymbol{V}_{nn}^{p} \end{bmatrix} \begin{Bmatrix} \boldsymbol{x}_0^p \\ \boldsymbol{x}_1^p \\ \vdots \\ \boldsymbol{x}_n^p \end{Bmatrix} = \begin{Bmatrix} \boldsymbol{H}_0^p \hat{\boldsymbol{q}}_0^p \\ \boldsymbol{H}_1^p \hat{\boldsymbol{q}}_1^p \\ \vdots \\ \boldsymbol{H}_n^p \hat{\boldsymbol{q}}_n^p \end{Bmatrix} \tag{7}$$

where superscripts p, subscripts 0 and $k, k = 1, \ldots, n$, stand for polymer, quantities associated exclusively with a domain, and quantities associated with the interface between the kth nanotube and the matrix, respectively. The submatrices $[\boldsymbol{U}]$, $[\boldsymbol{V}]$, and $[\boldsymbol{H}]$ are given as

$$U_{IJ} = \int_{\Gamma_s^J} \phi_I^s v_J(Q)\, d\Gamma \tag{8}$$

$$V_{IJ} = \int_{\Gamma_s^J} q_I^s v_J(Q)\, d\Gamma \tag{9}$$

$$H_{IJ} = \int_{\Gamma_s^J} \Phi_I(\mathbf{s}) v_J(Q)\, d\Gamma \tag{10}$$

where Γ_s^J is a regularly shaped local region around a given node $\mathbf{s}_J$, v_J is a weight function, and $\mathbf{s}$ is a field point on the boundary.

Similarly, for the kth nanotube domain, we have

$$\begin{bmatrix} \boldsymbol{U}_{00}^{t_k} & \boldsymbol{U}_{0i}^{t_k} \\ \boldsymbol{U}_{i0}^{t_k} & \boldsymbol{U}_{ii}^{t_k} \end{bmatrix} \begin{Bmatrix} \boldsymbol{x}_0^{t_k} \\ \boldsymbol{x}_i^{t_k} \end{Bmatrix} = \begin{Bmatrix} \boldsymbol{H}_0^{t_k} \hat{\boldsymbol{\phi}}_0^{t_k} \\ \boldsymbol{H}_i^{t_k} \hat{\boldsymbol{\phi}}_i^{t_k} \end{Bmatrix} \tag{11}$$

and

$$\begin{bmatrix} \boldsymbol{V}_{00}^{t_k} & \boldsymbol{V}_{0i}^{t_k} \\ \boldsymbol{V}_{i0}^{t_k} & \boldsymbol{V}_{ii}^{t_k} \end{bmatrix} \begin{Bmatrix} \boldsymbol{x}_0^{t_k} \\ \boldsymbol{x}_i^{t_k} \end{Bmatrix} = \begin{Bmatrix} \boldsymbol{H}_0^{t_k} \hat{\boldsymbol{q}}_0^{t_k} \\ \boldsymbol{H}_i^{t_k} \hat{\boldsymbol{q}}_i^{t_k} \end{Bmatrix} \tag{12}$$

where the superscript t_k stands for the kth nanotube and the subscript i indicates the quantities associated with the interface between the kth nanotube and the matrix.

At the interface between a nanotube and the polymer, both the temperature and heat fluxes must be continuous, i.e.,

$$\{\phi_k^p\} = \{\phi_i^{t_k}\} \tag{13}$$

and

$$\{\boldsymbol{q}_k^p\} = -\{\boldsymbol{q}_i^{t_k}\} \tag{14}$$

Using the continuity conditions, Eqs. (6), (7), (11), and (12) can be assembled into the following expression:

$$\begin{bmatrix} \boldsymbol{A}_{00}^p & \boldsymbol{A}_{01}^p & \mathbf{0} & \mathbf{0} & \cdots & \boldsymbol{A}_{0k}^p & \mathbf{0} & \mathbf{0} \\ \boldsymbol{U}_{10}^p & \boldsymbol{U}_{11}^p & -\boldsymbol{U}_{ii}^{t_1} & -\boldsymbol{U}_{i0}^{t_1} & \cdots & \boldsymbol{U}_{1k}^p & \mathbf{0} & \mathbf{0} \\ \boldsymbol{V}_{10}^p & \boldsymbol{V}_{11}^p & \boldsymbol{V}_{ii}^{t_1} & \boldsymbol{V}_{i0}^{t_1} & \cdots & \boldsymbol{V}_{1k}^p & \mathbf{0} & \mathbf{0} \\ \mathbf{0} & \mathbf{0} & \boldsymbol{A}_{0i}^{t_1} & \boldsymbol{A}_{00}^{t_1} & \cdots & \mathbf{0} & \mathbf{0} & \mathbf{0} \\ \vdots & \vdots & \vdots & \vdots & \ddots & \vdots & \vdots & \vdots \\ \boldsymbol{U}_{n0}^p & \boldsymbol{U}_{n1}^p & \mathbf{0} & \mathbf{0} & \cdots & \boldsymbol{U}_{nn}^p & -\boldsymbol{U}_{ii}^{t_n} & -\boldsymbol{U}_{i0}^{t_n} \\ \boldsymbol{V}_{n0}^p & \boldsymbol{V}_{n1}^p & \mathbf{0} & \mathbf{0} & \cdots & \boldsymbol{V}_{nn}^p & \boldsymbol{V}_{ii}^{t_n} & \boldsymbol{V}_{i0}^{t_n} \\ \mathbf{0} & \mathbf{0} & \mathbf{0} & \mathbf{0} & \cdots & \mathbf{0} & \boldsymbol{A}_{0i}^{t_n} & \boldsymbol{A}_{00}^{t_n} \end{bmatrix} \begin{Bmatrix} \boldsymbol{x}_0^p \\ \boldsymbol{x}_1^p \\ \boldsymbol{x}_i^{t_1} \\ \boldsymbol{x}_0^{t_1} \\ \vdots \\ \boldsymbol{x}_n^p \\ \boldsymbol{x}_i^{t_n} \\ \boldsymbol{x}_0^{t_n} \end{Bmatrix} = \begin{Bmatrix} \boldsymbol{H}_0^p \boldsymbol{d}_0^p \\ \mathbf{0} \\ \mathbf{0} \\ \boldsymbol{H}_0^{t_1} \boldsymbol{d}_0^{t_1} \\ \vdots \\ \mathbf{0} \\ \mathbf{0} \\ \boldsymbol{H}_0^{t_n} \boldsymbol{d}_0^{t_n} \end{Bmatrix} \tag{15}$$

where $[\boldsymbol{A}_{0k}^*]$, $k = 0, 1, \ldots, n$ and i, and $\{\boldsymbol{d}_0^*\}$ (* represents p or t_k) are formed by merging $[\boldsymbol{U}_{0k}^*]$ and $[\boldsymbol{V}_{0k}^*]$, and $\{\hat{\phi}_0^*\}$ and $\{\hat{\boldsymbol{q}}_0^*\}$ according to the known boundary conditions, respectively. For degrees of freedom with prescribed temperature, the related elements in $\{\hat{\phi}_0^*\}$ are selected for $\{\boldsymbol{d}_0^*\}$, and the corresponding rows of in $[\boldsymbol{U}_{0k}^*]$ are selected for $[\boldsymbol{A}_{0k}^*]$; otherwise, elements in $\{\hat{\boldsymbol{q}}_0^*\}$ are selected for $\{\boldsymbol{d}_0^*\}$, and the corresponding rows in $[\boldsymbol{V}_{0k}^*]$ are selected for $[\boldsymbol{A}_{0k}^*]$.

The set of Eq. (15) is solved for the unknown parameters $\boldsymbol{x}$ by the standard Gauss elimination solver, and then, by back-substitution into Eqs. (6), (7), (11), and (12), the boundary unknowns are obtained either on the interfaces or the external boundary surfaces. As demonstrated, the multidomain hybrid BNM is a boundary-only, meshless approach. No boundary elements are used for either interpolation or integration purposes. Therefore, it may alleviate the discretization difficulty to a large extent.

3. NUMERICAL RESULTS

The concept of a representative volume element has been widely used for conventional fiber-reinforced composites at the microscale [15]. Recently, Liu and Chen [16] applied it for the study of the CNT-based composites for their mechanical properties. In their study, a single nanotube with surrounding matrix material was modeled, with properly applied boundary and interface conditions to account for the effects of the surrounding materials. The RVE was then solved by the finite-element method. In the same way, Fisher et al. [17] analyzed the effects of the CNT waviness on the equivalent Young's modulus of the composites using an

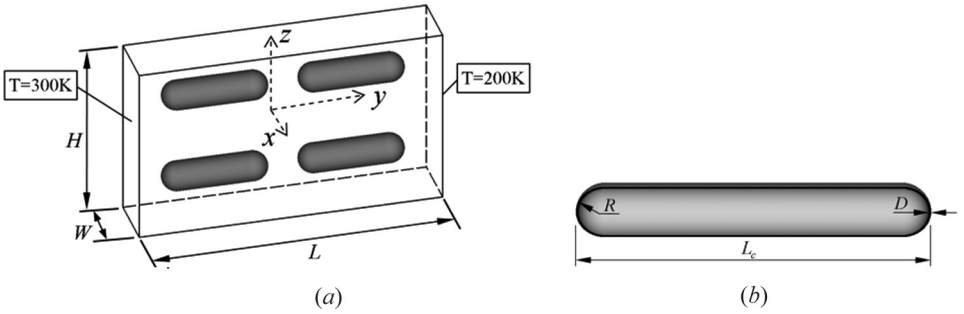

Figure 1. A nanoscale RVE and a CNT.

RVE containing a curved CNT. In this study, a rectangular RVE is selected, shown in Figure 1. The dimensions of the RVE are length $L = 100\,\text{nm}$, height $H = 60\,\text{nm}$, and width $W = 20\,\text{nm}$ (see Figure 1*a*). The CNTs are modeled as cylinder shells with two semisphere caps at each end (see Figure 1*b*), of which the outer radius $R = 5\,\text{nm}$, thickness $D = 0.4\,\text{nm}$ (which is close to the theoretical value of 0.34 nm for SWCNT thickness). The thicknesses and radii of the CNTs are identical to those of the semisphere caps, while their length L_c, together with the number of nanotubes and their alignments, varies for different examples. The heat conductivities used for the CNT and matrix (polycarbonate) are

CNT: $\kappa^t = 6{,}000\,\text{W/m K}$
Matrix: $\kappa^m = 0.37\,\text{W/m K}$

These values of the dimensions and material constants are within the wide ranges of those for CNTs reported in the literatures [1, 2].

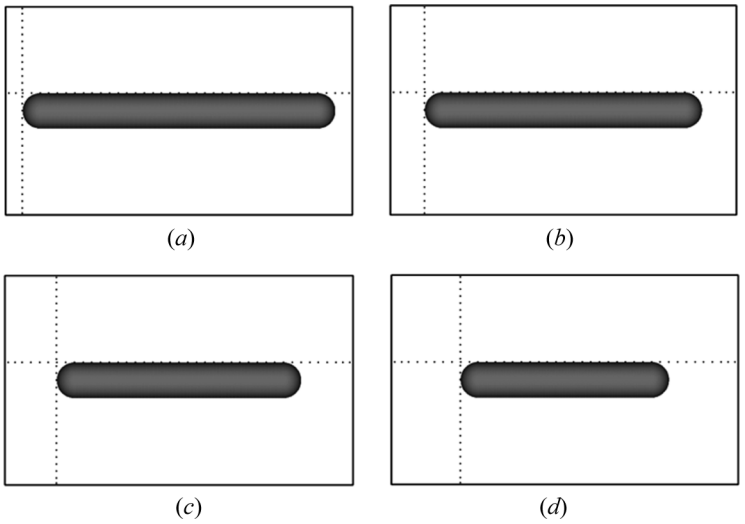

Figure 2. Nanoscale RVEs containing a single CNT.

Table 1. Equivalent heat conductivities for various CNT lengths

CNT length L_c (nm)	90	80	70	60
Volume fraction (%)	5.7	5.0	4.4	3.7
Conductivity (W/m K)	1.156	0.8619	0.6989	0.5919

Homogeneous boundary conditions are considered here, namely, uniform temperatures of 300 and 200 K imposed at the two end faces of the RVE, respectively, and heat flux free at the other four side faces. This boundary condition set allows us to estimate equivalent heat conductivity of CNT-based composite in the axial direction. Assuming homogeneous material properties and using Fourier's law, the formula for equivalent heat conductivity can be written as

$$\kappa = -\frac{qL}{\Delta\phi} \tag{16}$$

where κ represents the heat conductivity; q is the heat flux density, L is the length of the RVE in the axial direction, and $\Delta\phi$ is the temperature difference between the two end faces.

3.1. AN RVE CONTAINING A SINGLE NANOTUBE

An RVE with a straight nanotube embedded is first studied. The unit model is presented in Figure 2. Problems were solved for four lengths of the CNT, namely, 90, 80, 70, and 60 nm. In each case, 2,208 nodes are used for the CNT and 2,192 nodes for the matrix. Results for equivalent heat conductivity, together with volume fractions, are listed in Table 1.

Figure 3 presents the temperature distribution along the horizontally dotted lines (see Figure 2) all through the matrix. An obvious feature is observed that the

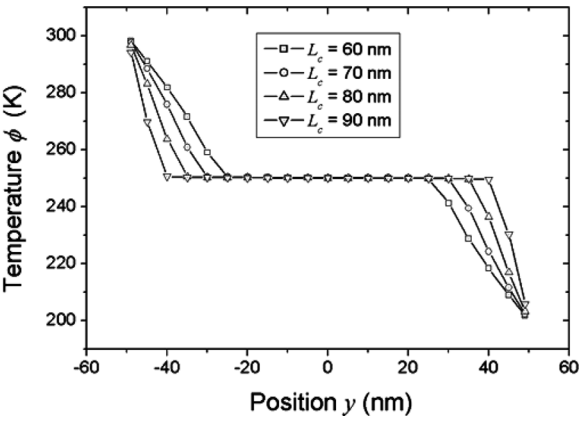

Figure 3. Temperature along the lines through the matrix.

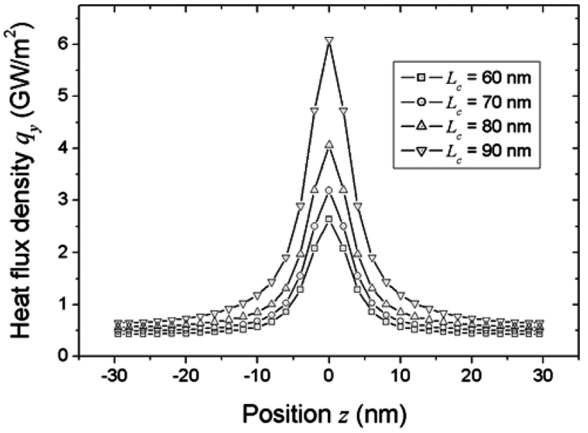

Figure 4. Heat flux distribution near the tip cap of the CNT.

temperature in the matrix first decreases from prescribed temperature value at an end face, then remains almost constant at the segments near the CNT, and finally continues to decrease to the lowest temperature at the other end face. This observation is consistent with the physical interpretation. Because the heat conductivity of the CNT is higher by several orders of magnitude than that of the matrix, almost the entire flux flows through the CNT. Therefore, almost no flux flows in the matrix in the segments near the CNT, and the temperature at these locations is almost uniform. The corresponding heat flux concentrations are also observed near the tips of the CNT in Figure 4. The curves in Figure 4 represent the heat fluxes in the y direction along the vertically dotted lines shown in Figure 2. It is seen that for longer CNTs, the concentration is higher. This result is consistent with that of the

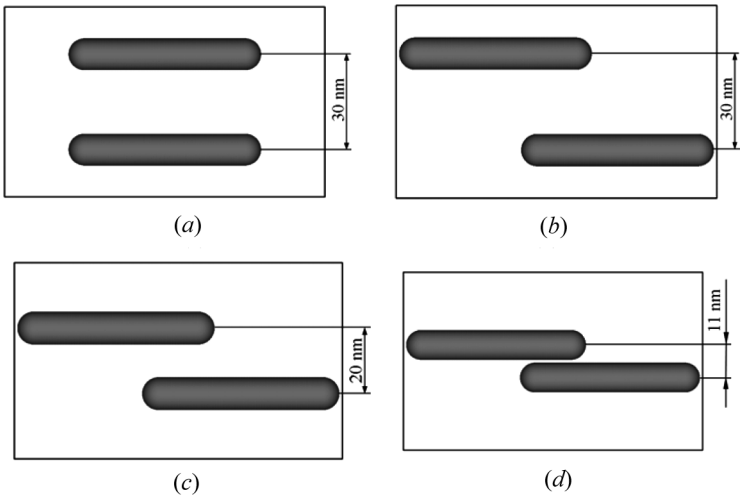

Figure 5. Nanoscale RVEs containing two CNTs.

Table 2. Equivalent heat conductivities for different CNT alignments

CNT alignment	(a)	(b)	(c)	(d)
Conductivity (W/m K)	0.7160	1.005	1.124	1.441

equivalent heat conductivity (listed in Table 1), that an RVE with a longer CNT embedded has a higher heat conductivity.

3.2. An RVE Containing Two Nanotubes

In this section, an RVE containing two CNTs of identical length is investigated. The CNT length equals 60 nm. Four alignments for the CNTs are considered, which are shown in Figure 5. The volume fractions of the CNTs for all four models are 7.4%. The equivalent heat conductivities for these RVEs are listed in Table 2. Among the four CNT alignments considered here, case (d) gives the highest value of equivalent heat conductivity, which is two times that of case (a). This means that the alignment of the CNTs in nanocomposites has a strong influence on their heat-conducting properties. Comparing the alignments (b), (c), and (d), it is found that the equivalent heat conductivity increases as the distance between the two CNTs decreases. The reason that alignment (d) gives the best result is that, in alignment (d), the two CNTs form a heat-conducting path which obviously reduces the heat-conducting resistance.

Figure 6 presents the temperature distribution along the horizontally dotted lines (see Figure 5) all through the matrix. Figure 7 shows the heat fluxes in the y direction along the vertically dotted lines shown in Figure 5. Again, the corresponding heat flux concentration occurs at the tips of the CNT. The amplitudes of the heat flux concentration for different alignments are consistent with the equivalent heat conductivities shown in Table 2. The alignment that gives a higher value of heat conductivity also leads to higher amplitude of flux concentration.

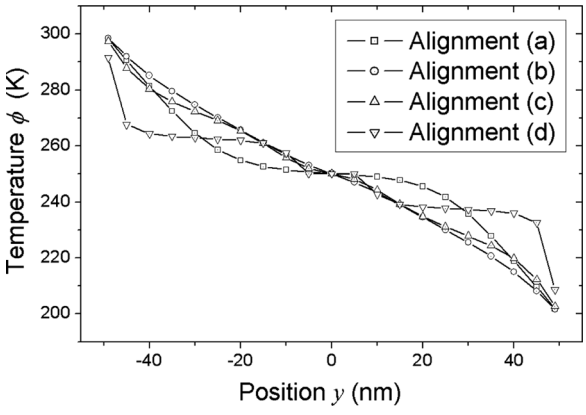

Figure 6. Temperature along the lines all through the matrix.

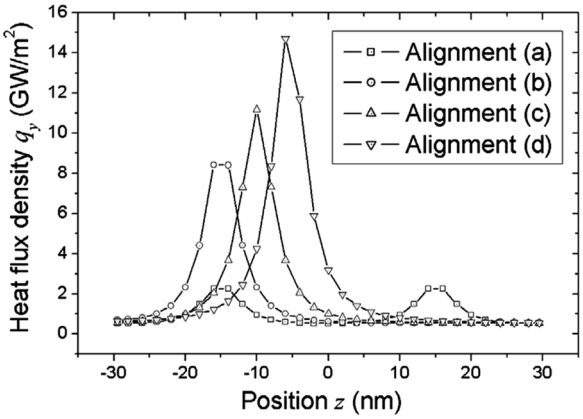

Figure 7. Heat flux distribution near the tip cap of the CNT.

3.3. An RVE Containing Four Nanotubes

In order to further study the effects of CNT dispersion and its influence on thermal properties of nanocomposites, an RVE model with four CNTs embedded is studied. Again, four different arrangements of the CNTs are considered, shown in Figure 8. The lengths of all four CNTs are 35 nm.

The volume fractions of the CNT for all four alignments are 8.3%. The equivalent heat conductivities of these RVEs are presented in Table 3. Once more, results show that the CNT dispersion has a great influence on the equivalent heat conductivity of the nanocomposites. As in the case of two CNTs, the highest heat conductivity is also obtained form alignment (d), while alignments (b) and (c) are close to each other and give the lowest values of the equivalent heat conductivity.

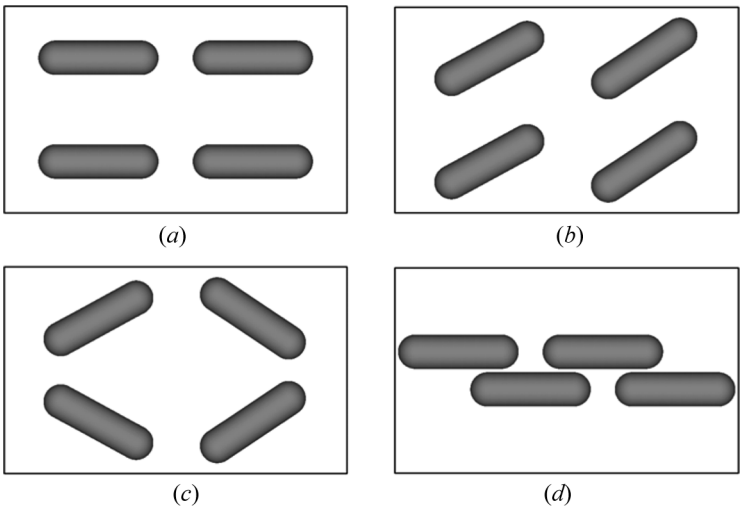

Figure 8. Nanoscale RVE containing four CNTs.

Table 3. Equivalent heat conductivities for different CNT alignments

CNT alignment	(a)	(b)	(c)	(d)
Conductivity (W/m K)	0.6974	0.5993	0.6015	0.9736

Temperature distribution along the horizontally dotted lines all through the matrix (see Figure 8) is presented in Figure 9. Comparing Figure 9 with Figures 6 and 3, it is seen that, in this model, the temperature decreases (from the highest value prescribed at one end face to the lowest value at other end face) more smoothly than in the models containing two or one CNT(s). This is because more and shorter CNTs are included in this RVE model and hence there are more homogenous properties. Figure 10 demonstrates the heat fluxes in the y direction along the vertically dotted lines shown in Figure 8. Again, among the four CNT alignments, the highest heat flux concentration occurs in alignment (d), which is consistent with the values of equivalent heat conductivity.

4. CONCLUSIONS

This article has presented a multidomain implementation of a hybrid BNM to the heat conduction analysis of CNT-based composites. The hybrid BNM is a meshless, boundary-only method requiring only discrete nodes located on bounding surfaces of the domain in question. Hence, it may greatly simplify the preprocessing and discretization tasks, making the approach extremely useful and more cost- and resources-effective than methods based on conventional FEM/BEM models.

The impact of the CNTs' dispersion on the equivalent thermal properties of the nanocomposites has been investigated through numerical simulation. Three RVEs containing one, two, and four nanotubes have been studied in detail. For each RVE, computations were performed for four kinds of CNT lengths (single CNT) or alignments (two or four CNTs). When the RVE contains a single CNT, the case for CNT length of 90 nm gives the highest value of equivalent heat conductivity,

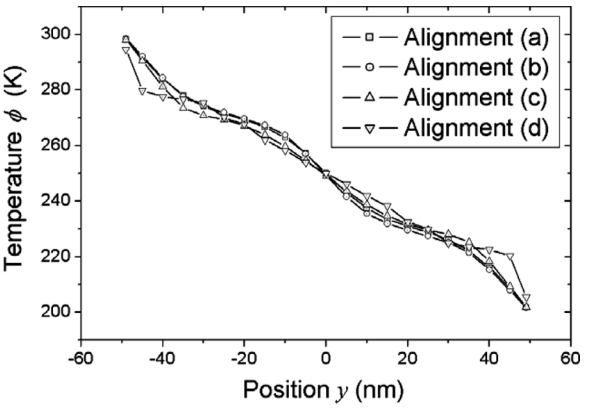

Figure 9. Temperature along the lines through the matrix.

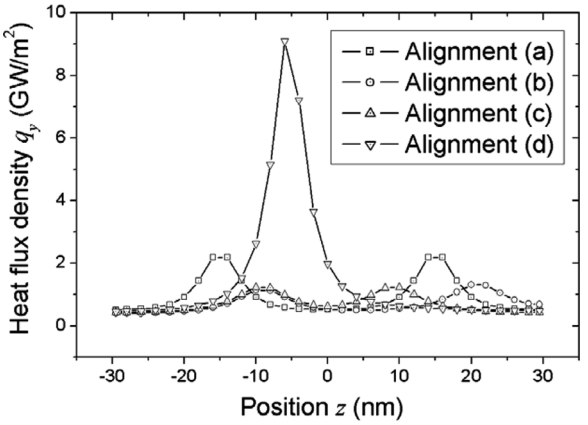

Figure 10. Heat flux distribution near the tip cap of the CNT.

which demonstrate that, with the addition of CNTs of about 5.7% (by volume fraction) to composites, the heat conductivity in the CNT axial direction can increase as much as 212%. For the RVEs containing two and four CNTs, results demonstrate that the equivalent thermal properties are strongly dependent on the CNT alignment. Some specific alignments may significantly increase the equivalent heat conductivity of the nanocomposites. From all the examples, it can be concluded that long CNTs are more effective than shorter CNTs in enhancing thermal properties of nanocomposites. Another interesting but perhaps a bit strange conclusion may be drawn, that the uniform dispersion of CNT gives the worst results.

REFERENCES

1. M. Endo, Y. A. Kim, K. Nishimura, T. Matushita, and T. Hayashi, From Vapor-Grown Carbon Fibers (VGCFs) to Carbon Nanotubes, in L. P. Biro, C. A. Bernardo, G. G. Tibbetts, and Ph. Lambin (eds.), *Carbon Filaments and Nanotubes: Common Origins, Differing Applications*, vol. 372, pp. 51–61, Kluwer, NATO Science Series E: Applied Sciences, Dordreoht, The Nehterlands, 2001.
2. M. Endo, Y. A. Kim, T. Hayashi, K. Nishimura, T. Matushita, K. Miyashita, and M. S. Dresselhaus, Vapor-Grown Carbon Fibers (VGCFs): Basic Properties and Their Battery Applications, *Carbon*, vol. 39, pp. 1287–1297, 2001.
3. J. Hone, M. Whitney, C. Piskoti, and A. Zettl, Thermal Conductivity of Single-Walled Nanotubes, *Phys. Rev. B*, vol. 59, pp. 2514–2516, 1999.
4. W. Yi, L. Lu, D. L. Zhang, Z. W. Pan, and S. S. Xie, Linear Specific Heat of Carbon Nanotubes, *Phys. Rev. B*, vol. 59, pp. 9015–9018, 1999.
5. S. Berber, Y. K. Kown, and D. Tomanek, Unusually High Thermal Conductivity of Carbon Nanotubes, *Phys. Rev. Lett.*, vol. 84, pp. 4613–4617, 2000.
6. D. Qian, E. C. Dickey, R. Andrews, and T. Rantell, Load Transfer and Deformation Mechanisms in Carbon Nanotube Polystyrene Composites, *Appl. Phys. Lett.*, vol. 76, pp. 2868–2870, 2000.
7. L. Jin, C. Bower, and O. Zhou, Alignment of Carbon Nanotubes in a Polymer Matrix by Mechanical Stretching, *Appl. Phys. Lett.*, vol. 73, pp. 1197–1199, 1998.

8. B. W. Smith, Z. Benes, D. E. Luzzi, J. E. Fischer, D. A. Walters, M. J. Casavant, J. Schmidt, and R. E. Smalley, Structural Anisotropy of Magnetically Aligned Single Wall Carbon Nanotube Films, *Appl. Phys. Lett.*, vol. 77, pp. 663–665, 2000.
9. D. Reneker and I. Chun, Nanometer Fibers of Polymer, Produce by Electrospinning, *Nanotechnology*, vol. 7, pp. 216–233, 1996.
10. J. M. Zhang, Z. H. Yao, and H. Li, A Hybrid Boundary Node Method, *Int. J. Numer. Meth. Eng.*, vol. 53, pp. 751–763, 2002.
11. J. M. Zhang and Z. H. Yao, Meshless Regular Hybrid Boundary Node Method, *Comput. Model. Eng. Sci.*, vol. 2, pp. 307–318, 2001.
12. J. M. Zhang, Z. H. Yao, and M. Tanaka, The Meshless Regular Hybrid Boundary Node Method for 2-D Linear Elasticity, *Eng. Anal. Boundary Elem.*, vol. 27, pp. 259–268, 2003.
13. J. M. Zhang and Z. H. Yao, Analysis of 2-D Thin Structures by the Meshless Regular Hybrid Boundary Node Method, *Acta Mech. Solida Sinica*, vol. 15, pp. 36–44, 2002.
14. J. M. Zhang, M. Tanaka, and T. Matsumoto, Meshless Analysis of Potential Problems in Three Dimensions with the Hybrid Boundary Node Method, *Int. J. Numer. Meth. Eng.*, vol. 59, pp. 1147–1160, 2004.
15. M. W. Hyer, *Stress Analysis of Fiber-Reinforced Composite Materials*, McGraw-Hill, Boston, 1998.
16. Y. J. Liu and X. L. Chen, Evaluations of the Effective Material Properties of Carbon Nanotube-Based Composites Using a Nanoscale Representative Volume Element, *Mech. Mater.*, vol. 35, pp. 69–81, 2003.
17. F. T. Fisher, R. D. Bradshaw, and L. C. Brinson, Effects of Nanotube Waviness on the Modulus of Nanotube-Reinforced Polymers, *Appl. Phys. Lett.*, vol. 80, pp. 4647–4649, 2000.